Cellular and Molecular Biology

Journal homepage: www.cellmolbiol.org

The Effect of Bromfenac Sodium Nanopolymer Used in Anterior Segment of the Eye on Corneal Neovascularization

Li Song[1], Xiao Liu[1], Nan Chen[2], Jiayan Liu[2], Aiqin Nie[3], Wei Li[3*]

[1]*Department of Ophthalmology, The First Affiliated Hospital of Jinan University, Guangzhou 510630, China*

[2]*Department of Ophthalmology, Panyu District, the Second Affiliated Hospital of Guangzhou Medical University, Guangzhou, 511447, China*

[3]*Department of Ophthalmology, The Second Clinical Medical College of Jinan University, Shenzhen 518000, Guangdong Province, China*

ARTICLE INFO

Original paper

Article history:
Received: December 01, 2021
Accepted: March 07, 2022
Published: March 31, 2022

Keywords:
bromfenac sodium/chitosan nanoparticles, corneal neovascularization, vascular endothelial growth factor, cyclooxygenase-2

ABSTRACT

This study was to explore the inhibitory effect of bromfenac sodium (BF) / chitosan (CS) nanoparticles (NPs) on corneal neovascularization (CNV). 45 New Zealand white rabbits provided by The First Affiliated Hospital of Jinan University were randomly divided into a control group (group A, n = 15), 0.1% BF aqueous solution treatment group (group B, n = 15), and 0.1% BF/CS-NPs suspension treatment group (group C, n = 15). A rabbit corneal alkali burn model was established. The average particle size of BF/CS-NPs with different BF concentrations was mainly 341.6 ± 12.9 nm - 548.7 ± 15.4 nm; and the Zeta potential distribution was 24.3 ± 2.5 mV - 35.7 ± 4.3 mV. When the initial concentration of BF was 1.5 mg/mL, the maximum drug loading was 57.35 ± 5.26%. The area of CNV in group C was significantly lower than that in groups B and A, and the differences were statistically significant ($P < 0.05$). At 6, 12, 18, and 24 days after surgery, the mRNA expression levels in cyclooxygenase-2 (COX-2) and vascular endothelial growth factor (VEGF) gene were compared after standardized by β-actin; group A had the highest expression level, followed by group B, and group C had the lowest expression level, showing statistically significant differences ($P < 0.05$). The BF/CS-NPs granules prepared in this study had stable physical and chemical properties and had a good sustained-release effect, and the release duration can be as long as 48 hours. BF/CS-NPs can inhibit the formation of CNV at different time points after alkali burn, and reduce the expression of VEGF and COX-2 in corneal tissue after alkali burn.

DOI: http://dx.doi.org/10.14715/cmb/2022.68.3.36

Introduction

Corneal neovascularization (CNV) can cause severe visual damage and even blindness, and it is also a high-risk factor for rejection after allogeneic keratoplasty. CNV occurs in about 1.4 million patients in the United States each year, and about 15% of them have a visual impairment (1, 2). At present, the treatment of CNV mainly uses local glucocorticoids and non-steroidal anti-inflammatory drugs and performs electrocoagulation, laser photocoagulation and photodynamic therapy on neovascularization. However, the clinical effects of these treatments did not meet expectations. In recent years, the research of drugs targeting molecules involved in the pathological mechanism of neovascularization, especially vascular endothelial growth factor (VEGF) drugs, has made great progress, and the therapeutic effects are also very satisfactory (3). Bromfenac sodium (BF) is also known as (2-amino-3-(4-bromobenzoyl)phenyl) sodium acetate. As a new generation of non-steroidal anti-inflammatory drugs, it has a unique chemical structure, making it a powerful anti-inflammatory drug, and also a lipophilic molecule that can penetrate eye tissues, thereby prolonging the duration of action (4-6). The strength of BF is 10 times that of other non-steroidal anti-inflammatory drugs. BF acting on the eyes can not only be anti-inflammatory and analgesic but also avoid the side effects of hormonal drugs. With the in-depth exploration of the pharmacological mechanism of BF, exciting new discoveries have been made in anti-angiogenesis, inhibition of retinal glial cell proliferation, and suppression of immune response. Especially in the field of optic nerve protection, BF also plays a very important function (7).

Studies have pointed out that the inhibitory effect

*Corresponding author. E-mail: liwei2022.com@yandex.com

of BF on inducible cyclooxygenase-2 (COX-2) is 3.7 times that of diclofenac. Because of the uniqueness and high efficiency of the inhibitory effect of BF on COX-2, BF has become an ocular agent for reducing ocular inflammation and neovascularization (8-10). A large number of studies have pointed out that BF aqueous solution has a good effect on the treatment of ocular inflammation and pain relief after cataract surgery, but there are few studies on the inhibitory effect of BF on CNV. In addition, BF has many problems in the treatment of ocular diseases, such as short drug duration, high dosing frequency, poor patient compliance, and the inability to obtain effective drug concentration in deep tissues of the eye (11, 12).

In recent years, with the rapid progress of nanotechnology, more and more scholars have begun to focus on nano-drug delivery systems. Nanoparticles (NPs) can not only improve the absorption of drugs and promote the bioavailability of drugs but also reduce the side effects of drugs and increase the duration of drug concentration in the eye. Chitosan (CS), also known as poly-2-amino-2-deoxy-β-D-glucose, is a biological macromolecule produced by the deacetylation reaction of chitin. It has many advantages, such as better biocompatibility, degradability, low immunogenicity, and non-toxicity, so it is widely used in various nano-drug delivery systems (13-15). In addition, the positive charge attached to the surface of CS can be closely combined with the negative charge in the ocular surface mucin layer to increase the force between molecules and enhance the mucosal adhesion of CS, thereby prolonging the adhesion time of the drug on the ocular surface and improving the bioavailability of BF.

Based on the above conditions, 60 New Zealand white rabbits were selected as experimental animals, and the prepared bromfenac sodium/chitosan nanoparticles (BF/CS-NPs) were applied in the rabbit CNV model to extend the stay and duration of action of BF on the ocular surface. The objective was to explore the inhibitory effect of BF/CS-NPs on rabbit CNV and provide a scientific experimental basis for the application of BF nanomedicine in ophthalmology.

Materials and methods

Testing animal grouping and modeling

45 New Zealand white rabbits were provided by the First Affiliated Hospital of Jinan University Animal Center, both male and female, with a weight of 2.0 - 2.5 kg. The animal experiment was approved by the First Affiliated Hospital of Jinan University Animal Ethics Committee, and the experimental process complied with the experimental guidelines of the Animal Ethics Committee.

A rabbit corneal alkali burn model was established. It could grasp the degree of rabbit corneal alkali burn according to the classification standard adopted by the Cooperative Research Group on Ocular Trauma and Occupational Eye Diseases (16). Before the experiment, a slit lamp microscope (Yunnan Yunao Optoelectronics Co., Ltd., China) was used to check and exclude corneal diseases, and the right eye was used as the test eye. After 3% sodium pentobarbital (Liaoning Dasheng Pharmaceutical Co., Ltd., China) intravenous anesthesia combined with 0.4% Obucaine Hydrochloride Eye Drops (Santian Pharmaceutical Co., Ltd., China) was adopted for anesthesia, a round filter paper with a diameter of 8 mm soaked with 1 mol/L NaOH solution was attached to the center of the rabbit's right cornea for 25s, and immediately washed with 0.9% sodium chloride aqueous solution repeatedly. After surgery, 0.3% tobramycin eye drops (Nanjing Pharmaceutical Factory Co., Ltd., China) were given to prevent infection. 45 rabbits were randomly divided into a control group (group A, n = 15), 0.1% BF aqueous solution treatment group (group B, n = 15), and 0.1% BF/CS-NPs suspension treatment group (group C, n = 15) using the random sampling method. Eye dropped once a day, 10 μL each time, for 24 days.

Preparation of BF/CS-NPs suspension

In this experiment, CS-NPs and BF/CS-NPs suspensions were prepared by the ion cross-linking method. Firstly, CS powder was added to 2% acetic acid (CH3COOH) solution to prepare 25 mL of 1.5 mg/mL CS acetic acid solution and stirred thoroughly. Under magnetic stirring, 10 mL of 1.0 mg/mL sodium tripolyphosphate (TTP) aqueous solution was placed dropwise to the CS acetic acid solution and continued stirring for 30 minutes at room temperature. When the solution appeared opalescent, it meant blank CS -NPs suspension was successfully prepared. Then, it could continue to prepare for the BF/CS-NPs suspension.

Before TPP was dropped into the chitosan acetic acid solution, different amounts of BF needed to be added to the above chitosan acetic acid solution to obtain concentrations of 0.3 mg/mL, 0.6 mg/mL, 0.9 mg/mL, 1.2 mg/mL, 1.5 mg/mL, 1.8 mg/mL, 2.1 mg/mL, 2.4 mg/mL, 2.7 mg/mL, and 3.0 mg/mL BF solution. The purpose of preparing the BF solution with no passing concentration was to study the effect of different initial concentrations of drugs on the physicochemical properties of drug-loaded CS-NPs. Finally, the prepared BF/CS-NPs suspension was centrifuged at 4°C and 15,000 r/min for 40 minutes, the supernatant was discarded, the precipitate was collected, and vacuum freeze-dried to obtain BF/CS-NPs freeze-dried powder.

Characterization analysis, encapsulation efficiency, and drug loading determination of BF/CS-NPs

After the BF/CS-NPs suspensions were prepared with different drug concentrations, the particle size and surface Zeta potential of the nanoparticles were measured using a laser particle size analyzer (Malvern Company, UK). After the BF/CS-NPs suspension was diluted with deionized water, it was dropped on the sample platform, fixed with conductive glue, and sprayed with gold. The voltage was increased to 5 kv, and then it was observed under an S-3400N scanning electron microscope (Hitachi, Japan). A small amount of diluted BF/CS-NPs suspension was dropped on a copper mesh covered with carbon film and placed at 25°C for 10 minutes. After natural drying, it was stained with 2% (w/v) phosphotungstic acid (Quzhou Ruierfeng Chemical Co., Ltd., China), and observed with a Tecnai-10 projection electron microscope (Philip Company, Netherlands). LC-2010AHT high-performance liquid chromatography (Shimadzu, Japan) was used to determine the content of BF in the supernatant.

The encapsulation efficiency and drug loading of nanoparticles could be calculated below equations:

Encapsulation rate = (BF total amount – BF content in supernatant)/BF total amount ×100% [1]

Drug loading = (total BF – BF content in the supernatant)/total mass of drug-loaded nanoparticles ×100% [2]

The concentration of BF in the sample was determined by reversed-phase high-performance liquid chromatography. The chromatogram was recorded. The cumulative release rate of the drug at each time point was calculated, including 4h, 8h, 12h, 16h, 20h, 24h, 28h, 32h, 36h, 40h, 44h, and 48h. The BF cumulative release rate-time curve was drawn according to the recorded results.

Observation of CNV

The slit-lamp microscope was used to observe rabbit CNV growth, congestion, edema and corneal opacity every day after surgery. The time for the growth of neovascular sprouts in the left and right eyes of each rabbit was recorded. CNV area was measured at 6d, 12d, 18d, and 24d after the surgery. The measurement mainly observed the longest blood vessel that had a small continuous curvature and grows toward the center of the corneal turbidity. The calculation equation of the CNV growth area was as follows:

$$N = \frac{C}{12} \times 3.1416 \times [R2 - (R - L) \times 2] \quad [3]$$

In equation [3], *N* represented the area of neovascularization; *C* represented the circumferential hour of the neovascularization involving the cornea; *R* = 6 mm, represents the corneal radius; and *L* referred to the length of the neovascularization extending from the limbus into the cornea.

At 6d, 12d, 18d, and 24d after surgery, the rabbits were anesthetized intravenously with 3% sodium pentobarbital and sacrificed by air embolism. The corneal tissue with a diameter of approximately 10 mm was removed from the right eye of each rabbit. A piece of corneal tissue was randomly selected from each group, fixed with 10% formaldehyde (Chengdu Kaida Chemical Trading Co., Ltd., China) solution for 24 hours, and embedded in paraffin. After tissue sectioning, hematoxylin-eosin (HE) staining was performed to observe the histopathological changes in the cornea. The remaining corneal tissue was detected by real-time fluorescent quantitative PCR (RT-qPCR) to determine the expression levels of COX-2 and VEGF genes in the experimental group and the control group.

RT-qPCR detection

The total ribonucleic acid (RNA) was extracted from rabbit corneal tissue. The corneal tissue was

ground with liquid nitrogen, transferred into a 1.5 mL EP tube, added with 1 mL of TRNzol (Beijing Biolab Technology Co., Ltd., China) to lyse on ice for 20 minutes. After that, the tissue was added with 0.2 mL of chloroform (Zibo Zengrui Chemical Co., Ltd., China) and mixed well. The tissue was centrifuged for 5 minutes at 4°C and 15,000 r/min to collect the supernatant. 450 μL of supernatant was transferred to EP tube, added with 450 μL of isopropanol and mixed well. Then, it was centrifuged at 4°C and 15000 r/min for 20 minutes to discard the supernatant, and the residual was added with 1 mL of pre-cooled 75% ethanol. Again, the solution was centrifuged at 15,000 r/min at 4°C for 5 minutes to discard the supernatant and added with 1 mL of absolute ethanol. After that, it was again centrifuged at 15,000 r/min at 4°C for 5 minutes to discard the supernatant and air dry for 10 minutes, and then dissolved in 40μL of 1‰ diethylpyrocarbonate (DEPC) water and stored in a freezer at -70°C.

The purity and concentration of RNA were detected with ultraviolet (UV)-2600/2700 UV-Vis spectrophotometer (Shimadzu, Japan). 2 μg RNA template was extracted, and complementary deoxyribonucleic acid (cDNA) was synthesized according to the operating instructions of the reverse transcription kit. SYBR Green I (TOYOBO, Japan) fluorescent dye method was used for RT-qPCR detection.

COX-2 and VEGF gene reaction system included 10 μL of 2 × SYBR Green, 0.5 μL of upstream and downstream primers, 2.0 μL of cDNA, and 7.0 μL of ddH2O. Three replicate holes were made for each sample. The reaction conditions were defined as follows: 95°C for 5 minutes; 93°C for 30s, 56°C for 30s, 72°C for 30s, 50 cycles; and 72°C for 10 minutes. The $2^{-\triangle\triangle CT}$ method was used to calculate the mRNA expression levels of COX-2 and VEGF in the three groups at different periods.

Statistical methods

In this study, SPSS 22.0 was used as the statistical analysis software for data processing for statistical analysis. A single-factor analysis of variance was used for comparison between multiple groups, and the measurement data were expressed as $\bar{x} \pm s$. The results were statistically significant when $P < 0.05$.

Results and discussion

Characterization results, encapsulation efficiency, and drug loading of BF/CS-NPs

Since the raw material of bromfenac sodium was yellow, the prepared BF/CS-NPs suspension was a light yellow opalescent suspension, and the freeze-dried powder was yellow granular. Both transmission electron microscopy (TEM) and scanning electron microscopy (SEM) observation results showed that BF/CS-NPs were spherical, with smooth surface, uniform dispersion, and no adhesion, and the average particle size was about 548.7 ± 15.4 nm (Figure 1).

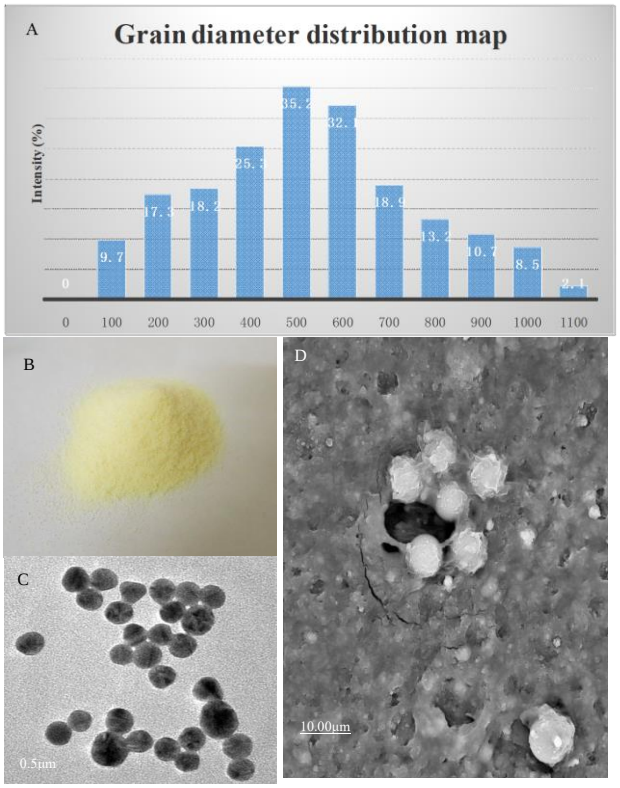

Figure 1. Characterization results of BF/CS-NPs. Note: Figure A showed the particle size distribution; Figure B showed the picture of BF/CS-NPs freeze-dried powder; Figure C was an image under TEM, and Figure D showed an image under SEM.

Figure 2 showed the characterization and determination results of BF/CS-NPs with different BF concentrations. The average particle size distribution range of BF/CS-NPs with different BF concentrations was relatively concentrated, mainly 341.6 ± 12.9nm - 548.7 ± 15.4 nm; and the Zeta potential distribution was 24.3 ± 2.5 mV - 35.7 ± 4.3 mV. No obvious linear correlation was found between the initial concentration of different BFs, the average particle

size, and the Zeta potential distribution. When the Zeta potential was positive, it was the BF/CS-NPs that can tightly combine with the negative charges in the rabbit corneal mucin layer, increasing the force and extending the duration of BF on the ocular surface.

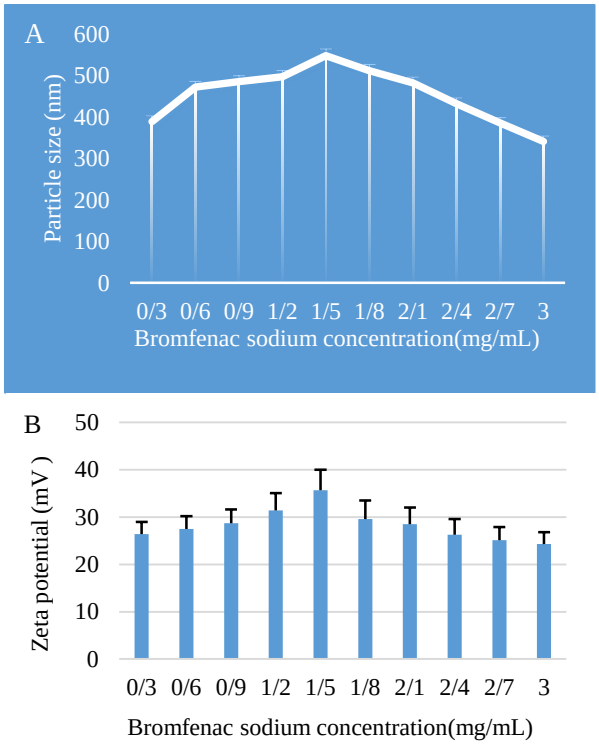

Figure 2. Characterization and determination results of BF/CS-NPs with different BF concentrations. Figure A and Figure B showed the average particle size and Zeta potential, respectively.

Figures 3 and 4 showed the encapsulation efficiency and drug loading of BF/CS-NPs with different BF concentrations. When the initial concentration of BF was 1.5 mg/mL, the drug loading was the maximum value of the experimental group 57.35 ± 5.26%. When the initial concentration of BF was 1.5 mg/mL, the increase in encapsulation rate tended to be flat, which was the best value in the experimental group (61.46 ± 2.75%). Figure 2-A and Figure 4 illustrated that the drug loading of BF/CS-NPs was positively correlated with the average particle size, which may be caused by the interaction between the positive charge on the surface of CS and the negative charge on the surface of BF. When the initial concentration of BF exceeded 1.5 mg/mL, the drug loading of nanomedicine reached a saturated state. Even if the drug concentration was increased, the drug loading of BF/CS-NPs would no longer increase. It was found in Figure 5 that at the initial release stage, BF/CS-NPs showed a very obvious burst release, it released 60% of the total BF in the first 24 hours, the release rate decreased after 32 hours of release, and the sustained release time could reach 48 hours.

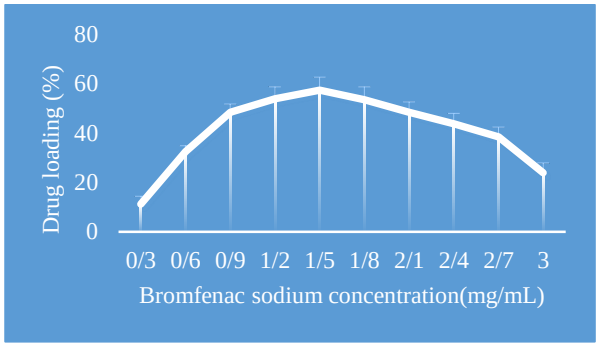

Figure 3. Encapsulation efficiency of BF/CS-NPs with different BF concentrations.

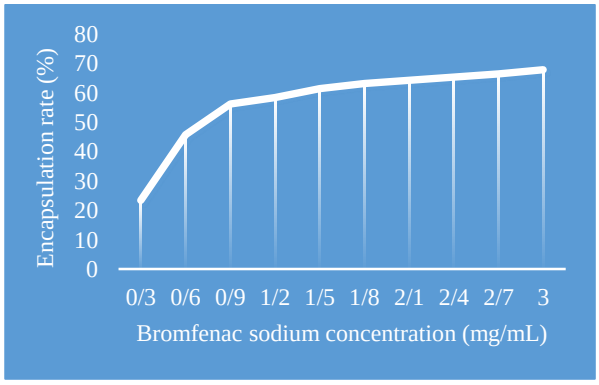

Figure 4. Drug loading of BF/CS-NPs with different BF concentrations.

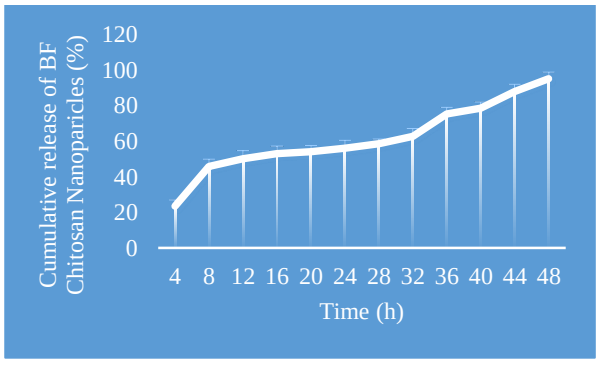

Figure 5. Cumulative release curve.

Rabbit CNV formation and pathological examination

After alkali burn, the rabbit cornea appeared grayish-white, dense and turbid, with clear boundaries. With time, the number, thickness, and

area of the three groups of CNV gradually increased. At each time point, the CNV areas of group B and group C were significantly lower than the area of group A, and the differences were statistically significant ($P < 0.05$); the CNV area of group C was significantly lower than that of group B ($P < 0.05$), as shown in Figure 6. It was fully confirmed that the experimentally prepared BF/CS-NPs had a good inhibitory effect on rabbit CNV.

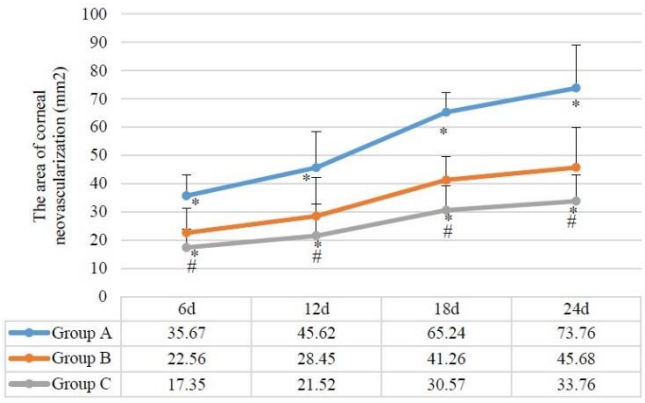

	6d	12d	18d	24d
Group A	35.67	45.62	65.24	73.76
Group B	22.56	28.45	41.26	45.68
Group C	17.35	21.52	30.57	33.76

Figure 6. Areas of the three groups of CNVs. Note: * and # indicated $P < 0.05$ compared with group A and group B, respectively.

The results of corneal histopathology showed that a large number of inflammatory cell infiltration and neovascularization were observed in group A, part of inflammatory cell infiltration was observed in group B, and a very small amount of inflammatory cells were observed in group C. Such results further confirmed that the BF/CS-NPs prepared in this experiment had anti-inflammatory effects, as shown in Figure 7.

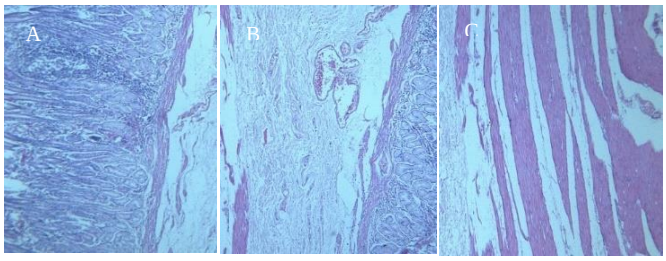

Figure 7. Histopathological sections of three groups of cornea 24 days after surgery. Note: image A showed that group A showed massive infiltration of inflammatory cells in the interstitium; image B showed group B was treated with 0.1% BF aqueous solution, and some inflammatory cell infiltration was seen, and image C showed the results of group C treated with 0.1% BF/CS-NPs, and there was only a small amount of inflammatory cell infiltration.

Corneal COX-2 and VEGF gene mRNA level detection results

The RT-qPCR amplification results of COX-2 and VEGF genes showed that the primers had good specificity and can be used for RT-qPCR detection. At 6, 12, 18, and 24 days after surgery, the three groups of COX-2 and VEGF gene mRNA expression levels were compared after they were standardized by β-actin. Group A had the highest expression level, followed by group B, and group C showed the lowest expression level. The differences at each time point in each group were statistically significant ($P < 0.05$), as illustrated in Figure 8.

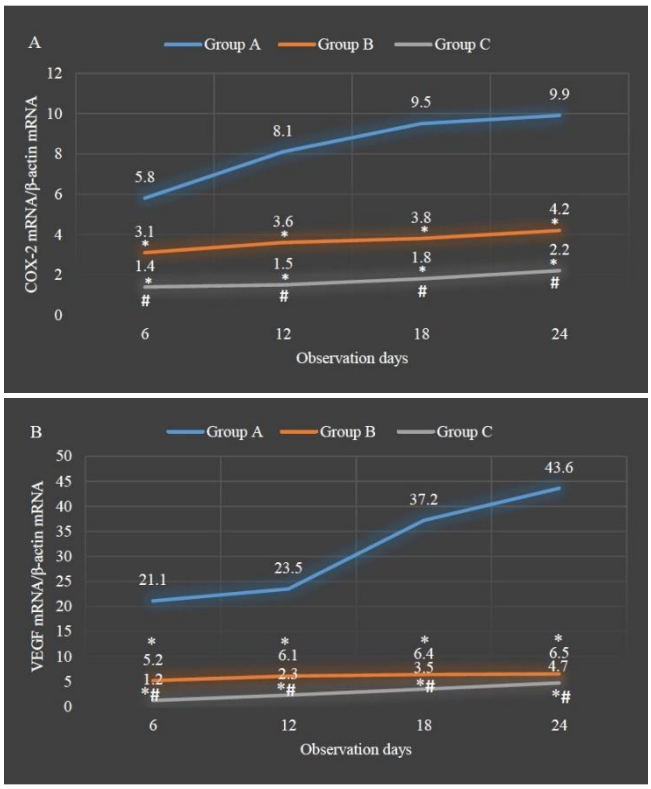

Figure 8. Comparison of RT-qPCR results of COX-2 mRNA and VEGF mRNA. Note: Figure A showed the RT-qPCR result of COX-2 mRNA; Figure B illustrated the RT-qPCR result of VEGF mRNA. * and # indicated $P < 0.05$ compared with group A and group B, respectively.

The production process of CNV is a very complicated pathological phenomenon, which includes not only the reorganization and dissolution of the original capillary basement membrane but also the expansion and metastasis of vascular endothelial cells. There are many cytokines involved in this production process, such as growth factors, interleukins, and angiogenins (17).

A nanoparticle carrier is a submicron drug carrier delivery system that belongs to the nanoscale and microscopic categories. In the past, many studies have shown that encapsulating drugs in nanoparticles can improve the biomembrane permeability of the drug, control the release rate of the drug, adjust the distribution range of the drug in the body, and improve the bioavailability of the drug (18-20). In this study, different initial concentrations of BF were adopted to screen out the best nanoparticles in all aspects. Then, the average particle size, Zeta potential, encapsulation efficiency, and drug loading were measured. It was found that nanoparticles with an initial BF concentration of 1.5 mg/mL were the best choice, and they were applied to the later rabbit CNV model. From the results of the drug release experiment of BF/CS-NPs, it was found that in the initial release stage, BF/CS-NPs had an obvious burst release phenomenon, and the drug release rate gradually slowed down as time passed. The burst release may be caused by the diffusion of BF adhered to the surface of nanoparticles (21). Zeta potential results showed that BF/CS-NPs had a positive charge on the surface in addition to their slow-release effect. When BF/CS-NPs were applied to the ocular surface of a rabbit model, they can be combined with the negative charge in the ocular surface mucin layer. The electrostatic interaction can not only increase the adhesion of BF/CS-NPs on the ocular surface but also expand the drug and cornea. The contact area of the surface increases the sustained action time of the drug on the ocular surface. Such results were similar to the results of Yang et al. (2020) (22). Therefore, the BF/CS-NPs prepared in this study can act on the target site for a long time and improve the bioavailability of the drug, which was in line with the initial experiment expectations.

Cyclooxygenase plays a key role in inflammation and can promote the conversion of arachidonic acid to prostaglandins. COX-2 is an inducible enzyme, which not only participates in various inflammatory reactions but also plays a role in the process of angiogenesis. Under various stimuli, its expression is slightly up-regulated (23-25). VEGF is closely related to the formation of new blood vessels. It can not only bind to receptors on the vascular endothelium to promote the division of endothelial cells, but also increase the permeability of blood vessels to promote endothelial cell transfer, dissolve the capillary basement membrane, and form new vascular lumen (26). The results of this experiment showed that in the corneal tissue after alkali burn, the number of new blood vessels increased during the gradual increase in corneal inflammation, and the mRNA levels of COX-2 and VEGF genes began to increase, and both showed a positive correlation. It indicates that COX-2 and VEGF are involved in the formation of corneal inflammation and CNV, and the up-regulation of COX-2 and VEGF may be related to the expression of their receptors.

BF is a highly selective inhibitor of COX-2. In the rabbit CNV model, its affinity for COX-2 is dozens of times that of ordinary COX. Therefore, the application of BF to the treatment of CNV has a good effect. In addition, the results of this experiment confirm that BF/CS-NPs have a significant inhibitory effect on the formation of CNV, which is consistent with the results of Wu et al. (2017) (27). In addition, the results of this study revealed that, compared with pure BF aqueous solution, BF was wrapped in CS-NPs, the biological effect of BF can be more lasting and more complete, and it can play a better suppression effect in the generation of CNV. The reason is that CS wraps BF in it, which produces a certain degree of protective effect on the drug, reducing the rate of degradation of BF by ocular surface lysosomes.

Conclusions

In this study, BF/CS-NPs were prepared and applied to the alkali burn rabbit CNV model to observe the characterization results of BF/CS-NPs and their inhibitory effect on CNV. BF/CS-NPs can be successfully prepared by the ion cross-linking method, which had stable physical and chemical properties and had a good sustained-release effect. The release duration can be as long as 48 hours. BF/CS-NPs can inhibit the formation of CNV at different time points after alkali burn, and reduce the expression of COX-2 and VEGF mRNA in the corneal tissue after alkali burn. The limitation of this study was that the properties of nano-level drugs were not very stable and were easily interfered with by external factors. If nano-level drugs were to be used in clinical applications, the storage method was still a problem to be solved, and further exploration was needed in the later stage. In conclusion, this study provided the

possibility for nanoparticle carriers as targeted drug carriers and provided a new direction for CNV molecular-level therapy.

Acknowledgments

Not applicable.

Interest conflict

The authors declare that they have no conflict of interest.

References

1. Sharif Z, Sharif W. Corneal neovascularization: updates on pathophysiology, investigations & management. Rom J Ophthalmol. 2019 Jan-Mar;63(1):15-22. PMID: 31198893; PMCID: PMC6531773.
2. Oguido APMT, Hohmann MSN, Pinho-Ribeiro FA, Crespigio J, Domiciano TP, Verri WA Jr, Casella AMB. Naringenin Eye Drops Inhibit Corneal Neovascularization by Anti-Inflammatory and Antioxidant Mechanisms. Invest Ophthalmol Vis Sci. 2017 Nov 1;58(13):5764-5776. doi: 10.1167/iovs.16-19702. PMID: 29117277.
3. Baradaran-Rafii A, Ashnagar A, Heidari Keshel S, Jabbehdari S, Baradaran-Rafii G. Regression of corneal neovascularization: Adiponectin versus bevacizumab eye drops. Eur J Ophthalmol. 2021 Jan;31(1):78-82. doi: 10.1177/1120672119874947. Epub 2019 Sep 15. PMID: 31523981.
4. Kasiri A, Mirdehghan MS, Farrahi F, Ostadian F, Feghhi M, Ghomi MR, Mohammad Jafari A, Mahdian Rad A, Kasiri N. Prevention of Corneal Neovascularization; a Preliminary Experimental Study in Rabbits. Med Hypothesis Discov Innov Ophthalmol. 2020;9(1):47-55. Epub 2020 Jan 1. PMID: 31976343; PMCID: PMC6969563.
5. Yu H, Sun L, Cui J, Li Y, Yan Y, Wei X, Wang C, Song F, Jiang W, Liu Y, Ge H, Qian H, Li X, Tang X, Liu P. Three kinds of corneal host cells contribute differently to corneal neovascularization. EBioMedicine. 2019 Jun;44:542-553. doi: 10.1016/j.ebiom.2019.05.026. Epub 2019 May 22. PMID: 31126890; PMCID: PMC6604366.
6. Wu P, Zhang D, Geng Y, Li R, Zhang Y. Circular RNA-ZNF609 regulates corneal neovascularization by acting as a sponge of miR-184. Exp Eye Res. 2020 Mar;192:107937. doi: 10.1016/j.exer.2020.107937. Epub 2020 Jan 16. PMID: 31954666.
7. Jin L, Zhang Y, Liang W, Lu X, Piri N, Wang W, Kaplan HJ, Dean DC, Zhang L, Liu Y. Zeb1 promotes corneal neovascularization by regulation of vascular endothelial cell proliferation. Commun Biol. 2020 Jul 3;3(1):349. doi: 10.1038/s42003-020-1069-z. PMID: 32620870; PMCID: PMC7335040.
8. Luis de Redín I, Boiero C, Recalde S, Agüeros M, Allemandi D, Llabot JM, García-Layana A, Irache JM. In vivo effect of bevacizumab-loaded albumin nanoparticles in the treatment of corneal neovascularization. Exp Eye Res. 2019 Aug;185:107697. doi: 10.1016/j.exer.2019.107697. Epub 2019 Jun 19. PMID: 31228461.
9. Wolf M, Clay SM, Zheng S, Pan P, Chan MF. MMP12 Inhibits Corneal Neovascularization and Inflammation through Regulation of CCL2. Sci Rep. 2019 Aug 9;9(1):11579. doi: 10.1038/s41598-019-47831-z. PMID: 31399604; PMCID: PMC6689067.
10. Mukwaya A, Mirabelli P, Lennikov A, Thangavelu M, Jensen L, Peebo B, Lagali N. Repeat Corneal Neovascularization is Characterized by More Aggressive Inflammation and Vessel Invasion Than in the Initial Phase. Invest Ophthalmol Vis Sci. 2019 Jul 1;60(8):2990-3001. doi: 10.1167/iovs.19-27591. PMID: 31310656.
11. Chen M, Bao L, Zhao M, Cao J, Zheng H. Progress in Research on the Role of FGF in the Formation and Treatment of Corneal Neovascularization. Front Pharmacol. 2020 Feb 25;11:111. doi: 10.3389/fphar.2020.00111. PMID: 32158390; PMCID: PMC7052042.
12. Wang X, Tang L, Zhang Z, Li W, Chen Y. Keratocytes promote corneal neovascularization through VEGFr3 induced by PPARα-inhibition. Exp Eye Res. 2020 Apr;193:107982. doi: 10.1016/j.exer.2020.107982. Epub 2020 Feb 21. PMID: 32092288.
13. Mukwaya A, Jensen L, Peebo B, Lagali N. MicroRNAs in the cornea: Role and implications for treatment of corneal neovascularization. Ocul Surf. 2019 Jul;17(3):400-411. doi: 10.1016/j.jtos.2019.04.002. Epub 2019 Apr 5. PMID: 30959113.
14. Barry Z, Park B, Corson TW. Pharmacological Potential of Small Molecules for Treating Corneal Neovascularization. Molecules. 2020 Jul 30;25(15):3468. doi: 10.3390/molecules25153468. PMID: 32751576; PMCID: PMC7435801.
15. Li H, Ye B, Zhu L, Wu L. Epigallocatechin gallate inhibits corneal neovascularization in ratalkaline burn model. Pak J Pharm Sci. 2018 May;31(3(Supplementary)):1087-1092. PMID: 29731448.
16. Yuan K, Zheng J, Huang X, Zhang Y, Han Y, Hu R, Jin X. Neutrophil extracellular traps promote corneal neovascularization-induced by alkali burn. Int Immunopharmacol. 2020 Nov;88:106902. doi: 10.1016/j.intimp.2020.106902. Epub 2020 Aug 20. PMID: 32829090.
17. Schaub F, Hou Y, Zhang W, Bock F, Hos D, Cursiefen C. Corneal Crosslinking to Regress Pathologic Corneal Neovascularization Before High-Risk Keratoplasty. Cornea. 2021 Feb 1;40(2):147-155. doi: 10.1097/ICO.0000000000002406. PMID: 33395116.
18. Haber A, Polania-Baron EJ, Bolaños-Jimenez R, Navas A, Graue Hernandez EO, Garfias Y. Analysis of CCR3 expression in corneal neovascularization in a murine model and human corneas. Exp Eye Res. 2020

Aug;197:108076. doi: 10.1016/j.exer.2020.108076. Epub 2020 May 30. PMID: 32485201.

19. Shen M, Zhou XZ, Ye L, Yuan Q, Shi C, Zhu PW, Jiang N, Ma MY, Yang QC, Shao Y. Xanthatin inhibits corneal neovascularization by inhibiting the VEGFR2‑mediated STAT3/PI3K/Akt signaling pathway. Int J Mol Med. 2018 Aug;42(2):769-778. doi: 10.3892/ijmm.2018.3646. Epub 2018 Apr 30. PMID: 29717775; PMCID: PMC6034915.
20. Liu H, Zhang XR, Xu HC, Ma Y, Huang LY, Zhai LY, Zhao Y. Effects of VEGF Inhibitor Conbercept on Corneal Neovascularization Following Penetrating Keratoplasty in Rabbit Model. Clin Ophthalmol. 2020 Jul 31;14:2185-2193. doi: 10.2147/OPTH.S260302. PMID: 32801629; PMCID: PMC7410491.
21. Aşula MF, Onur IU, Yigit FU. Efficacy of fumagillin bicyclohexylamine on experimental corneal neovascularization in rat model. Int Ophthalmol. 2019 Jul;39(7):1553-1558. doi: 10.1007/s10792-018-0964-5. Epub 2018 Jul 13. PMID: 30006905.
22. Yang J, Luo L, Oh Y, Meng T, Chai G, Xia S, Emmert D, Wang B, Eberhart CG, Lee S, Stark WJ, Ensign LM, Hanes J, Xu Q. Sunitinib malate-loaded biodegradable microspheres for the prevention of corneal neovascularization in rats. J Control Release. 2020 Nov 10;327:456-466. doi: 10.1016/j.jconrel.2020.08.019. Epub 2020 Aug 18. PMID: 32822742; PMCID: PMC8105765.
23. Bignami F, Lorusso A, Rama P, Ferrari G. Growth inhibition of formed corneal neovascularization following Fosaprepitant treatment. Acta Ophthalmol. 2017 Nov;95(7):e641-e648. doi: 10.1111/aos.13304. Epub 2017 Feb 15. PMID: 28205389.
24. Irani YD, Pulford E, Mortimer L, Irani S, Butler L, Klebe S, Williams KA. Sex differences in corneal neovascularization in response to superficial corneal cautery in the rat. PLoS One. 2019 Sep 3;14(9):e0221566. doi: 10.1371/journal.pone.0221566. PMID: 31479468; PMCID: PMC6719872.
25. Chu C, Yu J, Ren E, Ou S, Zhang Y, Wu Y, Wu H, Zhang Y, Zhu J, Dai Q, Wang X, Zhao Q, Li W, Liu Z, Chen X, Liu G. Multimodal Photoacoustic Imaging-Guided Regression of Corneal Neovascularization: A Non-Invasive and Safe Strategy. Adv Sci (Weinh). 2020 May 29;7(14):2000346. doi: 10.1002/advs.202000346. PMID: 32714751; PMCID: PMC7375239.
26. Nanji A, Redd T, Chamberlain W, Schallhorn JM, Chen S, Ploner S, Maier A, Fujimoto JG, Jia Y, Huang D, Li Y. Application of Corneal Optical Coherence Tomography Angiography for Assessment of Vessel Depth in Corneal Neovascularization. Cornea. 2020 May;39(5):598-604. doi: 10.1097/ICO.0000000000002232. PMID: 31868851; PMCID: PMC7179392.
27. Wu Y, Xue C, Lu Y, Huang Z. The inhibitory effect of different concentrations of KH902 eye drops on corneal neovascularization induced by alkali burn. Indian J Ophthalmol. 2017 Nov;65(11):1127-1132. doi: 10.4103/ijo.IJO_339_17. PMID: 29133637; PMCID: PMC5700579.